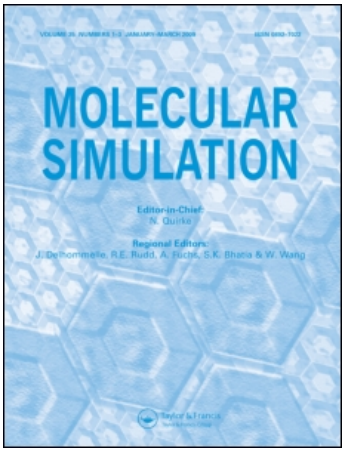

Molecular Simulation

Publication details, including instructions for authors and subscription information:
http://www.informaworld.com/smpp/title~content=t713644482

Ab initio simulations of the electrochemical activation of water

C. D. Taylor[a]; M. J. Janik[a]; M. Neurock[b]; R. G. Kelly[c]

[a] Department of Chemical Engineering, University of Virginia, Charlottesville, VA, USA [b] Department of Chemistry, University of Virginia, Charlottesville, VA, USA [c] Departments of Materials Science and Engineering, University of Virginia, Charlottesville, VA, USA

To cite this Article Taylor, C. D. , Janik, M. J. , Neurock, M. and Kelly, R. G.(2007) '*Ab initio* simulations of the electrochemical activation of water', Molecular Simulation, 33: 4, 429 — 436

To link to this Article: DOI: 10.1080/08927020601154207

URL: http://dx.doi.org/10.1080/08927020601154207

Molecular Simulation, Vol. 33, Nos. 4–5, 15–30 April 2007, 429–436

Taylor & Francis
Taylor & Francis Group

Ab initio simulations of the electrochemical activation of water

C. D. TAYLOR†, M. J. JANIK†, M. NEUROCK‡* and R. G. KELLY¶

†Department of Chemical Engineering, University of Virginia, Charlottesville, VA 22904-4741, USA
‡Department of Chemistry, University of Virginia, Charlottesville, VA 22904-4741, USA
¶Departments of Materials Science and Engineering, University of Virginia, Charlottesville, VA 22904-4741, USA

(Received June 2006; in final form October 2006)

First principles periodic density functional theory (DFT) has been applied to simulate the electrochemical interface between water and various (111) metal surfaces. The chemistry of water at these electrified interfaces is simulated and the parameters relevant to the macroscopic behavior of the interface, such as the capacitance and the potential of zero charge (PZC) are examined. In addition, we examine the influence of co-adsorbed CO upon the equilibrium potential for the activation of water over Pt(111). We find that for copper and platinum there is a potential window over which water is inert, but on Ni(111) water is always found in some dissociated form (as adsorbed OH* or H*, depending on the applied potential). Furthermore, the relaxation of water molecules via the flip/flop rotation is an important contribution to the interfacial capacitance. Our calculations for the coadsorbed H_2O/CO system indicate that the adsorption of CO affects the binding energy of OH, such that water activation occurs at a higher equilibrium potential.

Keywords: Electrochemistry; Density functional theory; Water activation; Metal surfaces

1. Introduction

The water/metal interface is critical to the performance of a number of chemical, biological and materials systems including electrocatalysts for fuel cells, corrosion-resistant metal alloys, electrochemically-deposited electronic and magnetic films, and inorganic scaffolds used for biomolecular adhesion. The reactivity and electrochemical behavior of the metal/solution interface is dictated by the explicit atomic and electronic structure that forms at the interface as a response to environmental conditions such as an applied potential [1]. Elucidating the structure and chemistry at this interface, however, is a considerable challenge due to the large number of molecular configurations that result from different water molecule orientations in the hydrogen bonded network, the presence or formation of ions and their positions within the interface and the potential reactions that can occur between these species [2]. The spectroscopic resolution of the molecular level transformations that occur at this interface as a function of applied electrochemical conditions is difficult to obtain. While theory has made important advances in elucidating gas-phase reactions on metal substrates, there have been very few *ab initio* studies of the electrified metal/solution interface [3–5]. These previous studies were pioneering, as they provided insights into the reactivity of the interface but were quite qualitative due to insufficient descriptions of the metal, solution and/or the potential. We recently developed an *ab initio* quantum mechanical approach based on density functional theory (DFT) to simulate the specific changes in the atomic structure of the water/metal interface and its reactivity as a function of applied potential [6,7].

The simulation of electrochemical systems from first-principles presents a significant challenge in that electrochemistry typically involves constant potential systems, for example in a fuel cell operating under steady state conditions, or in electrochemical deposition. Quantum mechanics, on the other hand, is typically carried out using constant electron models [8]. A true treatment of a constant potential system would require a full quantum mechanical simulation of the anode, cathode, ion transport across the membrane as well as electron conduction through the circuit. This is well outside the range of what is feasible. We have instead developed a half-cell approach whereby we simulate the electrode using periodic metal slabs together with condensed water, ions and an explicit charge to the metal. By charging the

*Corresponding author. Email: mn4n@virginia.edu

Molecular Simulation
ISSN 0892-7022 print/ISSN 1029-0435 online © 2007 Taylor & Francis
http://www.tandf.co.uk/journals
DOI: 10.1080/08927020601154207

Table 1. Charges (Q), potentials (U) and energies (E) for the various metal/adsorbate systems considered in this paper.

System	*Q*	*U*	*E*	*System*	*Q*	*U*	*E*
Cu(111)/H_2O	0	0.25	−452.70	Ni(111)/H_2O	0	0.07	−492.45
	−0.5	−0.49	−452.08		−0.5	−1.09	−491.56
	−1	−1.07	−451.97		−1	−1.89	−491.39
	0.5	0.78	−453.26		0.5	0.76	−493.28
	1	1.56	−454.63		1	1.57	−494.72
Cu(111)/OH	0	0.37	−453.23	Ni(111)/OH	0	0.04	−492.60
	−0.5	−0.28	−452.16		−0.5	−0.94	−490.90
	−1	−1.09	−451.12		−1	−1.74	−489.95
	0.5	1.21	−455.12		0.5	0.99	−494.80
	1	1.85	−456.98		1	1.82	−497.15
Cu(111)/O	0	0.39	−452.97	Ni(111)/O	0	−0.46	−490.39
	−0.5	−0.21	−451.33		−0.5	−1.32	−488.03
	−1	−1.14	−449.25		−1	−1.87	−486.89
	0.5	1.26	−455.86		0.5	0.31	−492.99
	1	2.02	−458.82		1	1.17	−496.26
Cu(111)/ H	0	0.34	−451.52	Ni(111)/ H	0	0.24	−492.29
	−0.5	−0.17	−451.67		−0.5	−0.64	−492.53
	−1	−0.81	−452.19		−1	−1.30	−493.07
	0.5	1.27	−451.74		0.5	1.20	−492.53
	1	1.99	−452.31		1	2.01	−493.17
Pt(111)/H_2O	−1	−1.16	−480.61	Pt(111)/CO/H_2O	−1	−1.22	−482.26
	−0.5	−0.62	−480.16		−0.5	−0.67	−481.82
	0	−0.04	−480.00		0	0.02	−481.64
	0.5	0.63	−480.18		0.5	0.61	−481.82
	1	1.18	−480.63		1	1.09	−482.25
Pt(111)/OH	−1	−1.55	−478.40	Pt(111)/CO/OH	−1	−1.21	−480.16
	−0.5	−0.99	−478.50		−0.5	−0.53	−480.33
	0	−0.31	−479.00		0	0.09	−480.78
	0.5	0.29	−479.77		0.5	0.71	−481.59
	1	0.70	−480.52		1	1.58	−483.02

metal we can induce an electric field across the aqueous/metal interface which polarizes the water molecules and results in a specific potential drop. The potential at the interface along with the free energy of the system can be calculated through the use of a double referencing method [7]. The free energies for different surface species can then be mapped-out as a function of applied potential by applying different surface charges to the metal. As such, we can construct electrochemical phase diagrams which can be used to determine constant potential changes in overall reaction energies as well as activation barriers. The approach is used in this paper to examine the electro-oxidation and reduction of water over different metal substrates and to understand the different activities of these metals. In addition, we extend the approach to model an intermediate step involved in the oxidation of methanol, this being the activation of water in the presence of CO. This latter study is a continuation of previous studies modeling the chemistries of water and methanol [6,9] over metal surfaces.

2. Theoretical methods

The reaction environment of an aqueous electrocatalytic event is marked by two key features: (1) a change in the bonding arrangement of atoms at the electrode/solution interface, and (2) electron transfer. Both of these features are significantly controlled by the electrode potential, as surface field effects can alter molecular geometries, and the energy of the transferred electron is raised or lowered according to the relation:

$$E(\mathrm{e}^-) = |\mathrm{e}|(U - 4.6) \quad (1)$$

where the 4.6 V term comes from estimations of the H_2/H^+ equilibrium potential relative to the vacuum state (i.e. the work function of the equilibrium hydrogen electrode) [10].

The perturbation of molecular geometries of reactant, intermediate and product species may become important when the reaction involves chemisorption to the electrode surface. In this case, a fully self-consistent theory is required that takes the polarization of the electrode into account. We have recently developed a method [7] which considers this by explicitly polarizing the electrode by a predetermined charge, q. Within the periodic DFT slab formalism which is used to determine the electronic band structure of the electrode, this effectively introduces a surface charge density of $q/2A$ where q is the charge applied, and A is the area of the slab face. Within the electrolyte region this charge becomes screened by a homogeneous countercharge of uniform charge density $-q/V$ that is distributed across the entire supercell, where V is the simulation volume. Perturbations in the electrode potential induced by the applied charge are measured with reference to an assumedly fixed reference potential for the solution-phase far from the electrode.

$$U_q = \Delta\Phi|_{\mathrm{slab,solution}} - \Phi_{\mathrm{soln},0} \quad (2)$$

The reference potential, $\Phi_{soln,0}$, is determined via a work-function calculation on the uncharged electrode-adsorbate-aqueous phase system. Utilizing the approach given in equation (2) gives rise to a simulation cell that acts as a capacitor with total capacitance:

$$C = 16\pi\varepsilon/L \tag{3}$$

where L is the inter-slab spacing. Here ε refers to the dielectric constant of the medium employed in the simulation. In the work employed thus far [6,7,9], the inter-layer space has been completely saturated with molecular H_2O at a density of 1 g/cm^3. The dielectric constant is around 5 for this model, as the full dynamical relaxation of the water molecules is not explicitly taken into account [7], as could be achieved by performing a computationally expensive set of *ab initio* molecular dynamics simulations. Tailoring L and ε (for example, by modifying the water structure or utilizing other solvent molecules) therefore allows one to model a system with a reasonable value for the capacitance.

The energies can be made fully self-consistent by appropriately accounting for the energy of the charge and countercharge as follows:

$$E_q = E_{slab,q} - \int_0^q \langle V(q)\rangle \mathrm{d}q + qU_q \tag{4}$$

The first term is the electronic structure energy of the slab in the field of the charge and countercharge, the second term decouples the background energy for consistency with calculations at other potentials/charge environments, and the third term decouples the energy due to the applied charge, q, according to equation (1). We find in nearly all cases that the energetic response is quadratic with respect to the potential U_q. This is in accord with the expansion about the potential of zero charge (PZC):

$$E_q(U_q) = E_0 + 1/2C(U_q - U_0)^2 \tag{5}$$

Within this framework, therefore, it is possible to perform geometry optimizations and self-consistent energy calculations for various reactant, intermediate and product species bound to an electrode in an electrocatalytic system, and to make thermodynamic predictions with regards to reaction mechanisms and allowable states in certain potential ranges.

The supercell geometry which is shown in figure 1 is used here to model the electrocatalytic activation of water over the close-packed surfaces of Cu(111), Pt(111) and Ni(111). Water may become activated to form a series of three products:

$$H_2O^* + e^- \rightarrow H^* + OH^- \tag{6}$$

$$H_2O^* \rightarrow OH^* + H^+ + e^- \tag{7}$$

$$H_2O^* \rightarrow O^* + 2H^+2e^- \tag{8}$$

The reactant and product states for equations (6)–(8) are shown in figure 2(a)–(d).

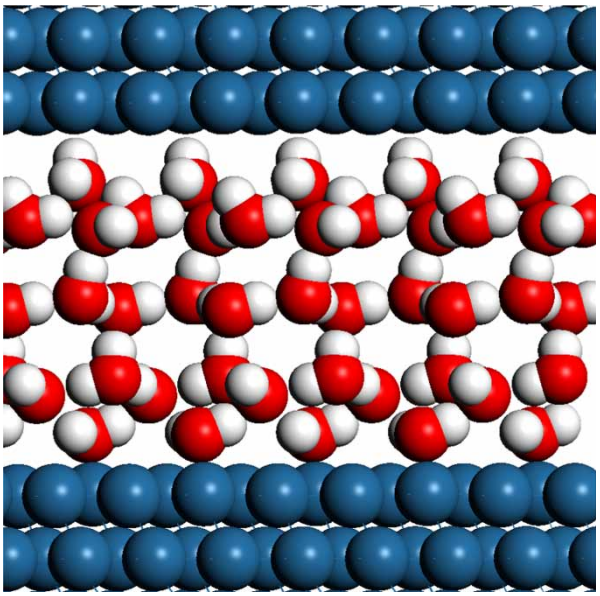

Figure 1. Supercell system used to describe the metal/solution interface in Model 3. Three supercells are shown in profile. Coordinates are given in supporting information.

The calculations of the electronic structure and geometry optimizations were performed using the PW91 [11] functional for Cu(111) and, in later work, RPBE [12] for Ni(111) and Pt(111). A 3 × 3 unit cell with three metal layers and the middle layer fixed at bulk positions were used. The program VASP [13–16] was used for all calculations. The energies of the systems are then calculated at potentials corresponding to surface charges of −15 through to +15 μC/cm^2.

The electron density is described using plane waves with a kinetic-energy cutoff of 396.0 eV, determined by oxygen. In all cases the ion cores are described using ultra-soft pseudopotentials [17] developed using the PW91 [11] correlation and exchange approximations. The Brillouin zone is sampled using a grid of 3 × 3 × 1 Monkhorst-Pack special k-points for all adsorbate structures [18]. Electronic SCF cycles are converged to 1.0×10^{-5} eV and the geometry was converged to 1.0×10^{-5} eV for quasi-Newton and conjugate-gradient optimizations. Partial occupancies of the wave-function are allowed by including order-two Methfessel–Paxton smearing [19] at a width of 0.2 eV.

For calculations of equations (7)–(9) over Cu(111) and Ni(111) the various states may involve the exchange of a proton or an electron. For these cases, the energy is corrected according to the energy of H^+(aq), via:

$$E(H^+(aq) = E(H) + \text{I.P.}(H) + \Delta E_{solv}(H^+(g)) \tag{9}$$

ΔE_{solv} is estimated from calculated ΔH values [20].

In the case of water activation over Pt(111) the energies of the excess proton and electron produced in equations (6)–(8) were incorporated as a function of potential, U_q, using a separate method. In this case we have made use of

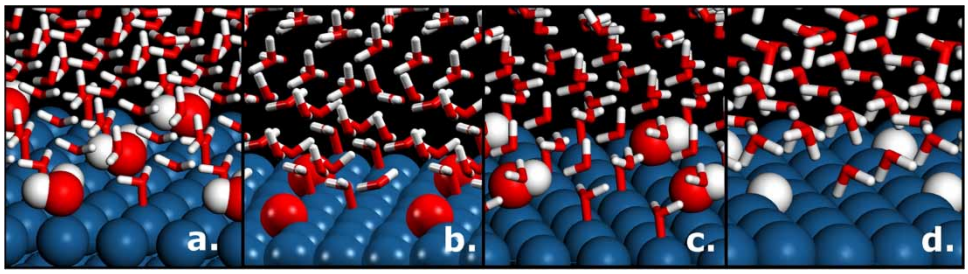

Figure 2. Snapshots indicating the adsorption geometry of: (a) water, (b) oxygen, (c) hydroxyl and (d) hydrogen for the neutral slabs utilized in Model 3.

the relation:

$$G_{\mathrm{H^+ + e}}(U_q) = 1/2G_{\mathrm{H2}} - \mathrm{e}U_q$$

Zero-point vibrational energy corrections to the total energy are applied as calculated under zero charge conditions (no applied potential) for the vibrational modes associated with the adsorbates, according to the data given in the appendix. Entropy terms are included for the vibrational entropy associated with the adsorbates, such that all energies stated are free energies computed at 300 K, as calculated by others [21].

The co-adsorption of CO and H_2O over Pt(111) was chosen such that one of the surface water molecules in the double layer structure over the Pt(111) surface is replaced with CO. This gives an effective coverage of 2/9 H_2O and 1/9 CO, with respect to the metal atoms. CO is shifted to the three-fold hollow site. This is a common problem for density functional predictions [22] for CO over Pt(111). We have not considered higher levels of theory to test the preference of CO for atop versus three-fold in the presence of the solvent environment (H_2O). Although this latter point may be important, the computational complexity involved is best left to a separate study. The three-fold hollow site minimizes the repulsive interactions of CO with the second water layer, as the regular hydrogen bonding network of the ice-like layer does not provide for stabilization of the CO adsorbate. The water density is optimized for the pure water calculation by minimizing the energy with respect to the length of the lattice vector normal to the surface (z-axis), as described above. This lattice vector is kept constant for all other calculations. For the calculation of water activation energies, a water molecule bound atop to a Pt atom and adjacent to the CO-adsorbed three-fold hollow site is converted to OH. The OH species remains atop the same Pt atom. The hydrogen atom removed for the water did not participate in hydrogen bonding prior to removal.

3. Results and discussion

We first evaluate the energy versus potential relation for the Cu(111)/H_2O model represented in figure 1. Two sets of calculations were carried out: one with the positions of all atoms fixed, and so only the electronic response to the applied potential could be observed; and one in which the positions of all atoms were allowed to relax. In this way the change in capacitance due to rotational molecular water reorientation could be directly observed. The resulting plot of energies versus potentials is shown in figure 3. It can be seen that allowing the water molecules to relax leads to a sharpening of the interfacial capacitance $\mathrm{d}^2E/\mathrm{d}U^2$ from 9.75 to 17.1 μF/cm^2. This corresponds to an effective increase of the dielectric constant for the modeled water array from $\sim$4.0 to 7.1, which is consistent with the interfacial dielectric constant assumed in traditional electrochemical theories [1].

Relaxed calculations were then performed for both the Ni(111)/H_2O and Cu(111)/H_2O interfaces, including the dissociation products in figure 2. The E versus U diagrams are parabolic in nature, due to the constant capacitance appearing within each of the individual phases. Changes in capacitance ultimately result in experimental studies due to changes in surface adsorption and specific/non-specific ion adsorption, which are here constrained as model dependencies within this framework. A superposition of such states (i.e. with different adsorption environments, etc.) would reflect these changes in capacitance. The E versus U plot for inactivated Ni(111)/H_2O is shown in figure 4. The PZC and the differential capacitance derived

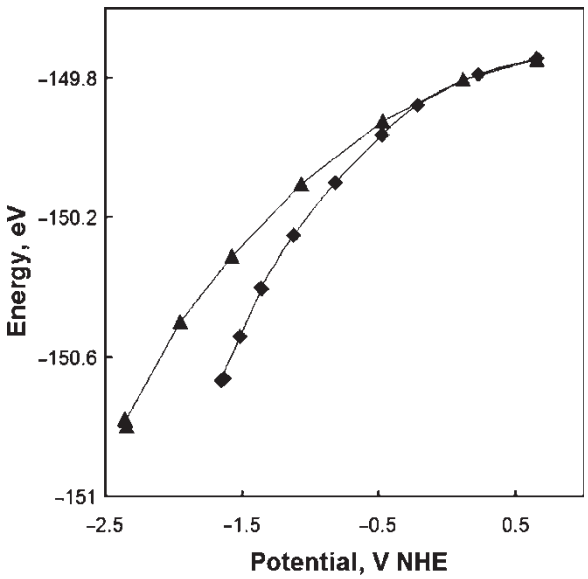

Figure 3. The free energy verses potential relation for the Cu(111)/H_2O interface when no molecular relaxation is allowed (triangles), and when molecular relaxation is allowed (diamonds).

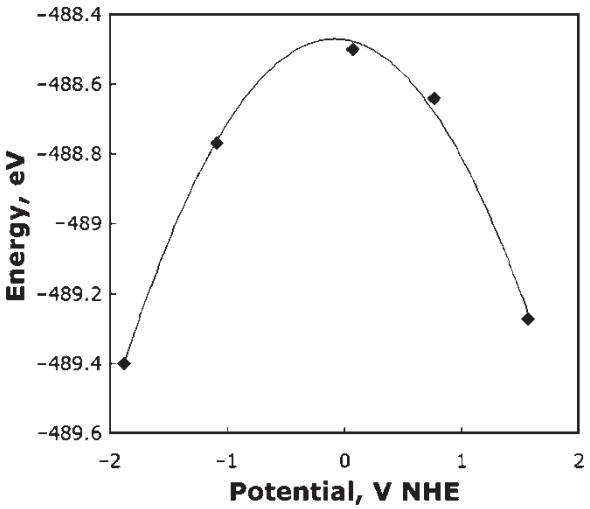

Figure 4. Energy diagram for water on Ni(111). Filled diamonds are DFT data points and the curve is a quadratic fit to the data used in determining the capacitance. Data points are given in table 1.

from this curve are -0.25 V NHE and 9.0 μF/cm^2, respectively. The experimental PZC of Ni(111) is -0.02 V NHE [23]. Interfacial capacitances for clean metal/solution interfaces have been estimated [24] at $\sim$15 μF/cm^2. The difference of 0.2 V in the PZC is within the acceptable range of the model at this level of fidelity. Indeed, it is to be expected that the 0 K static system will not reproduce dynamic quantities such as the PZC, where experimental estimates are averages over macroscopic time and length scales. Other studies performed in our group [25], and also by Halley and Price [26,27], have shown that the PZC does indeed fluctuate dramatically over the scale of picoseconds.

The diagrams for OH, H and O can be superposed upon the diagram for H_2O to show comparative energies. The resulting "phase-diagrams" for water over Ni(111) and water over Cu(111) are given in figure 5(a),(b), respectively.

The capacitances for the various adsorbed phases can been inferred from the curvature of the plots for the Ni(111)/H_2O interface in figure 5a. Adsorbed hydrogen has a substantially-lower interfacial capacitance of 4.8 μF/cm^2 compared to 9.0 μF/cm^2 for Ni(111)/H_2O, indicating that the adsorption of hydrogen reduces the capacity of the interface to retain charge. The adsorbed hydroxyl and oxygen phases have roughly the same capacitances as Ni(111)/H_2O (9.3 μF/cm^2 for OH and 11.2 μF/cm^2 for O). Adsorbed oxygen leads to a slight increase in the system capacitance, as it can effectively "hold" more surface charge.

The differences between the curves in figure 5 represent reaction energies and these differences are plotted for Ni(111)/H_2O in figure 6. Figure 6 also includes an indication of the perturbation to the system energies induced by changing the chemical potential of the released proton (the pH). This is accomplished by adding the standard chemical potential term to the reaction energy expression that treats pH:

$$(\mu)_{\mathrm{H}} = RT \ln([\mathrm{H}+])$$

The phase diagram for Ni(111)/H_2O is in accord with both theoretical predictions [28] that indicate that H_2O films have a thermodynamic propensity to dissociate over Ni(111), and electrochemical observations that suggest a region of co-adsorption of both H* and OH* on the electrode surface [29].

From figure 6 we see that the differences in capacitance between H_2O, OH, H and O phases make a negligible contribution to the energy differences as a function of potential, since the graphs are essentially linear. This is a reflection of the Gibb's relations for equations (6)–(8):

$$\Delta E(U) = \Delta E(U = 0) + nFU \tag{10}$$

By utilizing the expansions of equation (5) for the energy terms we can derive an alternative expression for $\Delta E(U)$, which directly incorporates the changes in the interface due to shifts in capacitance, surface charge density or molecular rearrangement at the interface. We do this

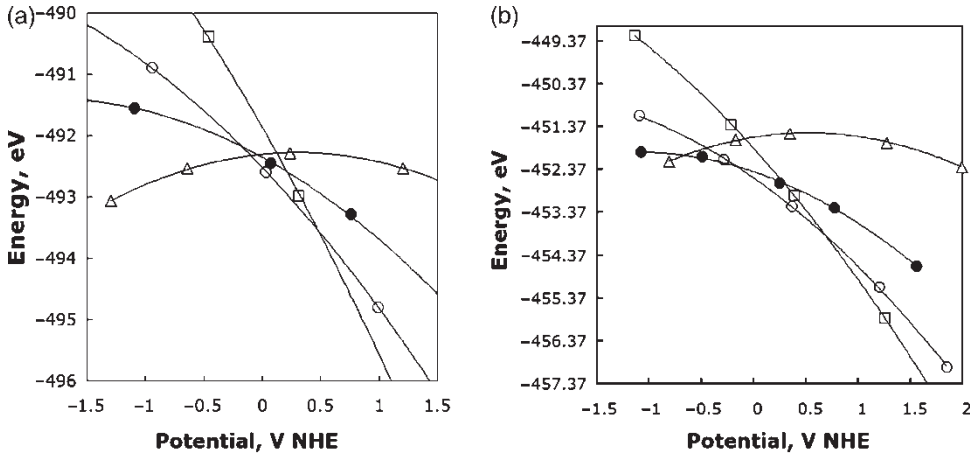

Figure 5. Phase diagram for surface hydride (open triangles), molecular water (solid circles), hydroxyl (open circles) and oxy species (open squares) on (a) Ni(111), and (b) Cu(111). Data points are given in table 1.

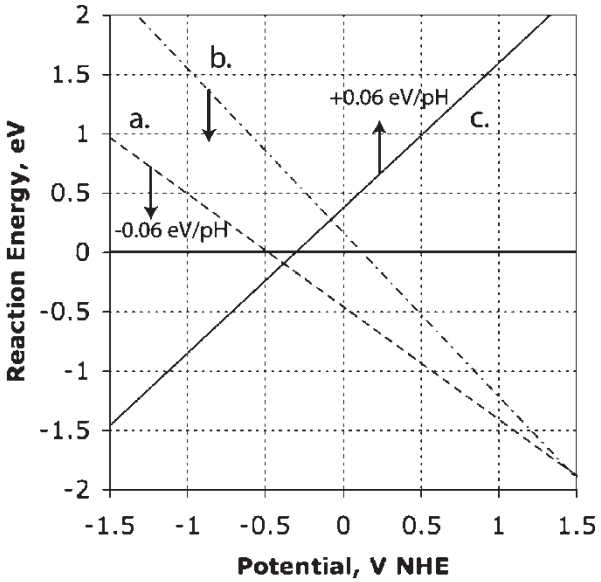

Figure 6. Reaction energies for (a. dashed) the 1-electron activation of water to produce hydroxyl, (b. dot-dashed) the 2-electron activation of water to oxygen overlayers and for (c. solid) the 1-electron activation of water to produce a hydrogen overlayer on Ni(111). The plotted curves are calculated at pH 0, and may be shifted according to pH as shown on this figure (b. shift, not shown for clarity, moves down by -0.12 eV/pH unit).

explicitly here for reaction (6):

$$\begin{aligned}\Delta E(U) &= E_{\mathrm{H}}(U) - \left(E_{\mathrm{H_2O}}(U) + E\left(\mathrm{H}^+_{(\mathrm{aq})} + \mathrm{e}U\right)\right.\\ &= E_{\mathrm{H,pzc}} + 1/2\mathrm{C_H}(U - U_{\mathrm{pzc,H}})^2\\ &\quad - \left(E_{\mathrm{H_2O,pzc}} + 1/2\mathrm{C_{H_2O}}(U - U_{\mathrm{pzc,H_2O}})^2\right.\\ &\quad \left.+E\left(\mathrm{H}^+_{(eq)}\right) - \mathrm{e}U\right) \qquad (11)\\ &= \left[E_{\mathrm{H,pzc}} - E_{\mathrm{H_2O,pzc}} + E\left(\mathrm{H}^+_{(\mathrm{aq})}\right) + 1/2\mathrm{C_H}U_{\mathrm{pzc,H^2}}\right.\\ &\quad \left.+ 1/2\mathrm{C_{H_2O}}U_{\mathrm{Pzc,H_2O^2}}\right] + [\mathrm{C_H}U_{\mathrm{pzc,H}} - \mathrm{C_{H_2O}}U_{pzc,\mathrm{H_2O}}\\ &\quad + \mathrm{e}]\mathrm{U} + 1/2[\mathrm{C_{H_2O}} - \mathrm{C_H}]U^2\end{aligned}$$

(12)

This form is more complex than the Gibb's relation (10) as it allows for perturbations in the capacitance to add second-order effects to the reaction thermodynamics, and perturbations in the PZC to affect the quantity of electrons transferred. This can be interpreted in the context of microscopic shifts in the electron density at the surface required to perform surface reactions in a constant potential way. PZC change upon surface adsorption in a manner similar to the work function shifts induced by adsorption [30,31]. In the case of figure 6, the linear terms are 1.22 for equation (6), 0.95 for equation (7) and 2.33 for equation (8). The deviation from Gibb's behavior is due to the PZC and capacitance shifts between adsorption phases as described above. A linear term of 0.95 for equation 7 indicates that upon activating water to form OH + H^+ + e^- over Ni, a 1 electron Faradaic current is generated, however, a reverse 0.05 electron non-Faradaic current is needed to maintain a constant potential. Alternatively, this can be thought of as indicating that activation of water generates only 0.95 electrons as 0.05 electrons must remain at the metal–hydroxyl interface. Thirdly, this can be stated that, in a formal charge sense, if water was assumed to be a neutral ligand, hydroxyl maintains a -0.05 charge. All of these statements correspond to formalistic ways to interpret adsorption and reaction behavior at the interface.

Finally, we have considered the case of water activation over Pt(111) in the presence of CO. This last study provides an example of moving to more complex co-adsorption scenarios as would be experienced in any practical electrode assembly. We examine here CO as a coadsorbate whereby one water molecule at the surface is removed and replaced by CO. In figure 7 we have shown the comparison between water activation curves ($H_2O \rightarrow OH + H^+ + e^-$) both with and without the coadsorbed CO. It is found that CO shifts the water activation equilibrium potential substantially to the right, from 0.48 V NHE to 1.29 V NHE, a shift of $\sim$800 mV. The co-adsorption of CO has little effect on the PZC or capacitance of the water–metal interface. However, analysis of the phase diagrams shows that CO affects the electrostatic environment of the hydroxyl–metal interface by shifting the PZC to more positive potentials and decreasing the capacitance. The capacitance is reduced as CO lacks the rotational response exhibited by the water dipole, as shown in figure 3. The PZC for the product state shifts by 0.35 V, which may be due to a synergetic effect between OH electron donation to the surface, and the receipt of electrons by the CO via back donation. Measurement of the electron density localized on the surface metal atoms indicates that the co-adsorption of CO leads to a reaction product with reduced electron transfer to the surface metal atoms. Not surprisingly, there is a greater deviation noted for the product state curves (CO/OH + H^+ + e^-) than for the reactant states (CO/H_2O), which is likely due to the interaction between the strongly bound CO and OH species,

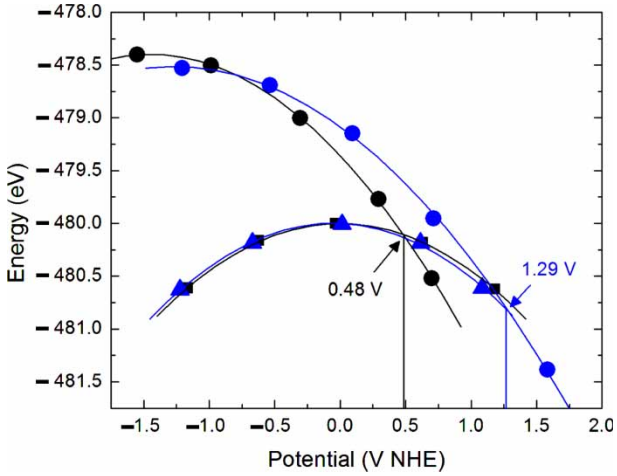

Figure 7. (Color) Water activation in the presence (blue) or absence (black) of CO. The activation potentials are indicated at the intersection points for each system (with and without CO). Data points are listed in table 1. Triangles and squares refer to molecular water whereas the circle refer to the adsorbed hydroxyl (colour in online version).

whereas H_2O is less tightly bound and so less subject to through-surface effects. Water activation leads to a slight repulsion of CO from the surface (increase in Pt—CO bond length of 0.02 V NHE), as it competes with OH for stronger adsorption to the surface. The donating ability of CO is reduced by the co-adsorption of the strongly bound, electron donating OH ligand, which correlates with the fact that the distance of CO from the surface is indicative of the magnitude of electron donation from CO [32]. Water on the other hand, is weakly bound, and so is not strongly affected by the presence of the CO. Hence the phase diagram for the reactant state has a PZC shift of only 0.07 V.

Experimentally, CO stripping voltammetry [33] also indicates that CO oxidation occurs at potentials more positive than that of water activation over pure Pt. A saturated layer of CO hinders water activation, even though saturation coverage is less than a complete monolayer (i.e. the hindrance is not purely steric in nature). Although not performed at the same coverage as our model, the basic thesis concurs with the concept of a local inhibition of water activation in the region adjacent to adsorbed CO. Note that our system likely produces an overstated shift in the water activation potential in the presence of CO due to the use of a single, static water structure.

4. Conclusions

By modeling reactions at the electrified water/metal interface using DFT within the framework of the Grand Canonical ensemble, it is possible to investigate the effects of molecular reorientation and electron transfer upon electrochemical thermodynamics. The energetic response of the electrochemical interface demonstrates quadratic behavior with respect to potential and was thus fit to a quadratic form, with the second-order term arising from the capacitance of the interface. The response of water molecules was shown to increase the system capacitance as water molecules can rotate, which effectively increases their dielectric constant and allows the interface to therefore contain more surface charge with shifts in electrochemical potential. The second-order term does not appear to contribute to changes in elementary reaction energies as a function of potential for the reactions examined here as the difference in polarization of reactant and product systems are predominantly due to the polarization of water. The second-order term is significantly smaller than the remaining linear terms arising from the Gibb's contribution and extra terms arising from non-Faradaic electron transfer which is required to maintain a constant electrochemical potential. Electrocatalytic processes involving more complex species, such as co-adsorbed CO and water, have also been treated with this method, and follow similar theoretical principles. CO is shown to have a through-surface effect on OH adsorption, leading to a shift in the electron donation properties of the bond, which is manifested by a change in the PZC. This work opens the way towards further simulation of complex environments at the electrochemical interface.

Acknowledgements

We gratefully acknowledge the financial support for this project from Department of Energy—Basic Energy Sciences, Center for Synthesis and Processing on Localized Corrosion, K. Zavadil, Lockheed-Martin Corporation (Ed Richey and George Young) and the Army Research Office for the MURI grant DAAD19-03-1-0169, and in addition the computational support from Environmental Molecular Sciences Laboratory at Pacific Northwest National Lab for computational resources. We would also like to thank Professor Jean Sebastian Filhol and Professor Sally Wasileski for invaluable discussions.

References

[1] J.O.M. Bockris, A.K.N. Reddy, M. Gamboa-Aldeco. *Modern Electrochemistry*, ed., Vol. 2A, Kluwer Academic/Plenum Publishers, New York (2000).
[2] C.D. Taylor, M. Neurock. Theoretical insights into the structure and reactivity of the aqueous/metal interface. *Curr. Opin. Solid State Mat. Sci.*, **9**, 49 (2006).
[3] A.B. Anderson, R. Kotz, E. Yeager. Theory for C-N and Ag-C vibrational frequency dependence on potential: Cyanide on a silver electrode. *Chem. Phys. Lett.*, **82**(1), 130 (1981).
[4] A.B. Anderson, N.C. Debnath. Mechanism of iron dissolution and passivation in an aqueous environment: Active and transition ranges. *J. Am. Chem. Soc.*, **105**, 18 (1983).
[5] A.B. Anderson, D.B. Kang. Quantum chemical approach to redox reactions including potential dependence: Application to a model for hydrogen evolution from diamond. *J. Phys. Chem. A.*, **102**, 5993 (1998).
[6] J.-S. Filhol, M. Neurock. Elucidation of the electrochemical activation of water over Pd by first principles. *Angew. Chem. Int. Ed. Engl.*, **45**, 402 (2006).
[7] C.D. Taylor, S.A. Wasileski, J.-S. Filhol, M. Neurock. First principles reaction modeling of the electrochemical interface: Consideration and calculation of a tunable surface potential from atomic and electronic structure. *Phys. Rev. B.*, **73**, 165402 (2006).
[8] A.Y. Lozovoi, A. Alavi, J. Kohanoff, R.M. Lynden-Bell. *Ab-initio* simulation of charged slabs at constant chemical potential. *J. Chem. Phys.*, **115**(4), 1661 (2001).
[9] D. Cao, G.-Q. Lu, A. Wieckowski, S.A. Wasileksi, M. Neurock. Mechanisms of methanol decomposition on Platinum: A combined experimental and ab-initio approach. *J. Phys. Chem. B.*, **109**, 11622 (2005).
[10] H. Reiss, A. Heller. The absolute potential of the standard hydrogen electrode: A new estimate. *J. Phys. Chem.*, **89**, 4207 (1985).
[11] J.P. Perdew, J.A. Chevary, S.H. Vosko, K.A. Jackson, M.R. Pederson, D.J. Singh, C. Fiolhais. Atoms, molecules, solids, and surfaces: Applications of the generalized gradient approximation for exchange and correlation. *Phys. Rev. B.*, **46**, 6671 (1992).
[12] B. Hammer, L.B. Hansen, J.K. Nørskov. Improved adsorption energetics within density functional theory using the revised Perdew-burke-Ernzerhof functional. *Phys. Rev. B.*, **59**, 7413 (1999).
[13] G. Kresse, J. Furthmuller. Efficient iterative schemes for ab-initio total-energy calculations using a planewave basis set. *Phys. Rev. B.*, **54**(16), 11169 (1996).
[14] G. Kresse, J. Furthmuller. Efficiency of *ab-initio* total-energy calculations for metals and semiconductors using a planewave basis set. *Comput. Mater. Sci.*, **6**, 15 (1996).
[15] G. Kresse, J. Hafner. *Ab-initio* molecular-dynamics simulation of the liquid-metal-amorphous-semiconductor transition in germanium. *Phys. Rev. B.*, **49**, 14251 (1994).
[16] G. Kresse, J. Hafner. *Ab-initio* molecular-dynamics for liquid-metals. *Phys. Rev. B.*, **47**, 558 (1993).
[17] D. Vanderbilt. Soft self-consistent pseudopotentials in a generalized eigenvalue formalism. *Phys. Rev. B.*, **41**, 7892 (1990).
[18] H.J. Monkhorst, J.D. Pack. Special points for Brillouin-zone integration. *Phys. Rev. B.*, **13**, 5188 (1976).

[19] M. Methfessel, A.T. Paxton. High-precision sampling for Brillouin-zone integration in metals. *Phys. Rev. B.*, **40**, 3616 (1989).
[20] J.A. Mejias, S. Lago. Calculation of the absolute hydration enthalpy and free energy of H^+, OH^-. *J. Chem. Phys.*, **113**(17), 7306 (2000).
[21] J.K. Nørskov, J. Rossmeisl, A. Logadottir, L. Lindqvist, J.R. Kitchin, T. Bligaard, H. Jonsson. The origin of the overpotential for oxygen reduction at a fuel-cell cathode. *J. Phys. Chem. B.*, **108**, 17886 (2004).
[22] R.A. Olsen, P.H.T. Philipsen, E.J. Baerends. CO on Pt(111): A puzzle revisited. *J. Chem. Phys.*, **119**(8), 4522 (2003).
[23] J. Sokolowski, J.M. Czajkowski, M. Turowska. Zero charge potential measurements of solid electrodes by inverse immersion methods. *Electrochim. Acta*, **35**, 1393 (1990).
[24] D.C. Grahame. The electrical double-layer and the theory of electrocapillarity. *Chem. Rev.*, **41**, 441 (1947).
[25] C.D. Taylor. First Principles modeling of the structure and reactivity of water at the metal/water interface Dissertation, University of Virginia, Charlottesville, January 2006.
[26] D.L. Price, J.W. Halley. Molecular-dynamics, density-functional-theory of the metal-electrolyte interface. *J. Chem. Phys.*, **102**(16), 6603 (1995).
[27] J.W. Halley, A. Mazzolo, Y. Zhou, D. Price. First principles simulations of the electrode-electrolyte interface. *J. Electroanal. Chem.*, **450**, 273 (1998).
[28] A. Michaelides, A. Alavi, D.A. King. Insights into H_2O-ice adsorption and dissociation on metal surfaces from first-principles simulations. *Phys. Rev. B.*, **69**, 113404 (2004).
[29] A. Saraby-Reintjes. Theory of competitive adsorption and its application to the anodic dissolution of nickel and other iron-group metals. *Electrochim. Acta*, **30**(3), 387 (1985).
[30] J.O.M. Bockris, S.D. Argade. Work functions of metals and the potential at which the have zero charge in contact with solutions. *J. Chem. Phys.*, **49**(11), 5133 (1968).
[31] S. Trasatti. Structure of the metal/electrolyte solution interface: New data for theory. *Electrochim. Acta*, **36**, 1659 (1991).
[32] S.A. Wasileksi, M.J. Weaver. What can we learn about electrode-chemisorbate bonding energetics from vibrational spectroscopy? An assessment from density functional theory. *Faraday Discussions*, **121**, 285 2002.
[33] H.A. Gasteiger, N. Markovic, P.N.J. Ross, E.J. Cairns. CO electrooxidation on well-characterized Pt-Ru alloys. *J. Phys. Chem.*, **98**, 617 (1994).